

AGP-based unitary coupled cluster theory for quantum computers

Armin Khamoshi*

Department of Physics and Astronomy, Rice University, Houston, Texas 77005, USA

Guo P. Chen†

Department of Chemistry, Rice University, Houston, Texas 77005, USA

Francesco A. Evangelista

*Department of Chemistry and Cherry Emerson Center for Scientific Computation,
Emory University, Atlanta, Georgia, 30322, USA*

Gustavo E. Scuseria‡

*Department of Chemistry, Rice University, Houston, Texas 77005, USA and
Department of Physics and Astronomy, Rice University, Houston, Texas 77005, USA*

(Dated: September 26, 2022)

Electronic structure methods typically benefit from symmetry breaking and restoration, specially in the strong correlation regime. The same goes for *Ansätze* on a quantum computer. We develop a unitary coupled cluster method based on the antisymmetrized geminal power (AGP)—a state formally equivalent to the number-projected Bardeen–Cooper–Schrieffer wavefunction. We demonstrate our method for the single-band Fermi–Hubbard Hamiltonian in one and two dimensions. We also explore post-selection as a state preparation step to obtain correlated AGP and prove that it scales no worse than $\mathcal{O}(\sqrt{M})$ in the number of measurements, thereby making it a less expensive alternative to gauge integration to restore particle number symmetry.

I. INTRODUCTION

One of the most sought after applications of quantum computers is to solve the strong correlation problem in electronic structure theory [1, 2]. Electronic structure methods often start from a mean-field state, typically a Hartree–Fock (HF) Slater determinant, and are systematically improved using a variety of techniques [3]. When electronic correlation is weak, single reference coupled cluster theory (CC) is known to be sufficiently accurate in quantum chemistry and is often regarded as the *gold-standard* [4, 5]. However, in the strongly correlated regime, many Slater determinants become equally dominant and single-reference methods often struggle [6].

Strong correlation in finite systems typically manifest itself by breaking one or more symmetries at the mean-field level. In this case, one could either make the mean-field state retain desired symmetries and correlate it in a *symmetry-adapted* manner, or, one could allow the symmetries to break and correlate the *symmetry-broken* mean-field state [7, 8]. The trade-off between these two strategies is that the broken symmetry wavefunction gives a lower energy at the expense of a less accurate wavefunction due to the lack of correct symmetries. This is known as the *symmetry dilemma* in electronic structure theory [9–12] and extends to traditional and unitary coupled cluster theory alike [13–15].

In recent years, there has been extensive interest in using physically inspired *Ansätze* in variational quantum algorithms [16]. In electronic structure calculations, the disentangled form of unitary CC (uCC) is perhaps the most natural extension of physically inspired *Ansätze* that can be implemented on a quantum computer [17–19]. For example, one can write down the uCC *Ansatz* as

$$|\psi(\vec{t})\rangle = \prod_k e^{t_k(\hat{\tau}_k - \hat{\tau}_k^\dagger)}|\phi\rangle, \quad (1)$$

where $|\phi\rangle$ is a mean-field reference, $\hat{\tau}_k$ is the k -th excitation operator which can be symmetry-adapted or broken, and t_k is the corresponding amplitude [20–22]. We can variationally minimize the energy,

$$E(\vec{t}) = \langle\psi(\vec{t})|H|\psi(\vec{t})\rangle, \quad (2)$$

using the variationally quantum eigensolver (VQE) in a hybrid quantum–classical optimization manner [23, 24]. To address the ambiguity in the ordering of the operators and the depth of the uCC *Ansatz*, heuristics such as the ADAPT-VQE [25] have been developed and extended over the years [26–28]. Other notable works along this direction are the qubit coupled cluster approach [29, 30], cluster-Jastrow *Ansatz* [31], k-UpCCGSD [32], and the projective quantum eigensolver (PQE) [33] among others [22, 34–37]. Combining VQE *Ansätze* with quantum Monte Carlo has been recently proposed as well [38].

An important consideration among all methods for noisy intermediate-scale quantum (NISQ) devices is how deep an *Ansatz* needs to be in order to achieve sufficient accuracy [39, 40] in the strongly correlated regime. For

* armin.khamoshi@rice.edu

† guo.chen@rice.edu

‡ guscus@rice.edu

example, when using a symmetry-adapted *Ansatz*, it is conceivable that more collective excitations are needed to recover the same level of accuracy in energy as those of symmetry-broken *Ansätze* in the regimes where symmetries break. This could require a larger number of variational parameters and deeper circuits to implement, which, in some cases, could scale exponentially.

A remedy for this problem could be to combine symmetry restoration with CC theory [14, 15, 41–44]. Symmetry breaking and restoration has long been studied in nuclear physics and electronic structure theory [7, 11, 12, 45]. It has also gained attention for applications on quantum computers in recent years. Restoration of parity, S^2 , S_z , translational, and other symmetries on a quantum computer have been proposed [46–53]. Some of the authors of this paper have shown how to efficiently restore particle number symmetry over the BCS wavefunction on a quantum computer [54]. The projected BCS wavefunction is known as the antisymmetrized geminal power (AGP) whose claim to fame is its ability to capture off-diagonal long-range order (ODLRO) without breaking number symmetry [55–57]. Common electronic structure methods, including HF and density functional theory, fail to capture ODLRO. Combining uCC with AGP is the central goal of this paper.

Number symmetry often breaks spontaneously for systems where the effective two-body interaction is attractive. The prime example is superconductivity or the superfluid phase in condensed matter and nuclear physics [58–60]. Number symmetry does not typically break in molecules [61]. However the AGP wavefunction has a long history in quantum chemistry as well, and it is connected to the concept of bonding [62]. AGP, by itself, is usually insufficient to accurately describe molecular systems, but it could be a good starting point for correlated methods such as configuration interactions or coupled cluster theory [63–68]. AGP-based quantum Monte Carlo methods have been used extensively over the years for molecules and solids [69–73]. Neuscamman has shown that variational Jastrow correlators on AGP is fully size-consistent and highly accurate [74, 75]. Ref. [31] developed a unitary analogue of this theory, although the authors were not aware of an efficient implementation of AGP on a quantum computer. Other geminal-based methods include using Richardson-Gaudin wavefunction [76–81], which although are not done on a quantum computer, they are relevant to AGP.

In Ref. [54] we demonstrated an efficient correlated AGP method on a quantum computer in the seniority-zero space. Our goal in this paper is to show how our previous formalism can be extended beyond seniority-zero systems and onto general *ab initio* Hamiltonians. To this end, we develop a unitary coupled cluster *Ansatz* atop of AGP and benchmark our numerical method against the ground state of the single-band Fermi–Hubbard model. The Hubbard Hamiltonian breaks number symmetry when the on-site interaction is attractive; and, when the on-site interactions is repulsive, it features strong corre-

lation prototypical of those that occur in molecules. Our intent is to demonstrate our method in both regimes of this Hamiltonian.

Another contribution of this paper is to exploit post-measurement selection, or *post-selection* in short, as an alternative to the $U(1)$ gauge integral in restoring number symmetry. Post-selection has been widely used as a crucial error mitigation technique for calculations performed on NISQ hardware [82–86]. We show, however, how post-selection can be used in conjunction with uCC to sample over correlated AGP. Our primary contribution is to show that restoring number symmetry with post-selection could scale more favorably than gauge integration as judged by the circuit depth and number of measurements. We analytically prove an asymptotic bound of $\mathcal{O}(\sqrt{M})$ measurements and confirm it with computations based on a noise-free quantum emulator.

Restoring symmetries via post-selection is a distinct possibility that is not viable on classical computers but can be conveniently performed on a quantum computer. Indeed, post-selection can be combined with the integral or phase estimation [50] to restore multiple symmetries. Our general philosophy for methods in strong correlation is to allow multiple symmetries to break and later restore them in the presence of the correlator. This could pave the way for methods that work equally well in repulsive, attractive, weak, and strong correlation regimes.

This paper is organized as follows: We begin Sec. II by first reviewing some previous work and basic concepts, then we build our way to seniority nonzero methods in Sec. II A. In Sec. II B, we discuss the optimization of AGP state on classical and quantum computers and review a formal connection with number projected HFB. Sec. II C is devoted to disentangled uCC on AGP. Sec. III discusses post-selection; the procedure is discussed in Sec. III A and the numerical benchmarks are presented in Sec. III B. In Sec. IV and the subsections therein, we demonstrate different uCC correlators based-on AGP and discuss our results for the Hubbard Hamiltonian. We conclude the paper with some final remarks in Sec. V.

II. THEORY

Define Γ^\dagger to be the geminal creation operator,

$$\Gamma^\dagger = \frac{1}{2} \sum_{pq} \eta_{pq} c_p^\dagger c_q^\dagger, \quad (3)$$

where c_p^\dagger is a fermionic creation operator in a spin-orbital p and η is an anti-symmetric matrix whose elements are known as the *geminal coefficients*. An AGP with N pairs, or $2N$ electrons, can then be defined as [56, 62]

$$|\text{AGP}\rangle = \frac{1}{N!} \left(\Gamma^\dagger\right)^N |\text{vac}\rangle. \quad (4)$$

Unless otherwise specified, we choose to work in the natural orbital basis of the geminal wherein the matrix η is

brought to a quasi-diagonal form [87],

$$\bar{\eta} = \bigoplus_{p=1}^M \begin{pmatrix} 0 & \eta_p \\ -\eta_p & 0 \end{pmatrix} = D^\dagger \eta D^*, \quad (5)$$

via the orbital rotation

$$a_p^\dagger = \sum_{q=1}^{2M} D_{qp} c_q^\dagger, \quad (6)$$

where D is the unitary matrix of natural orbital coefficients and M is the number of spatial orbitals. As such, the geminal operator can be written as

$$\Gamma^\dagger = \sum_{p=1}^M \eta_p a_p^\dagger a_{\bar{p}}^\dagger, \quad (7)$$

where the natural orbitals p and \bar{p} are ‘‘paired’’ in the sense of Eq. (5). As shown in Appendix A, a (p, \bar{p}) pair reduces to a spin (\uparrow, \downarrow) pair if the spins of the natural orbitals are collinear. With this pairing scheme, the relationship between AGP and the BCS wavefunction can be easily seen from

$$|\text{BCS}\rangle = \prod_{p=1}^M (u_p + v_p a_p^\dagger a_{\bar{p}}^\dagger) |\text{vac}\rangle \quad (8a)$$

$$\propto \prod_{p=1}^M (1 + \eta_p a_p^\dagger a_{\bar{p}}^\dagger) |\text{vac}\rangle \quad (8b)$$

$$= \sum_{N=0}^M \frac{1}{N!} (\Gamma^\dagger)^N |\text{vac}\rangle, \quad (8c)$$

where the BCS coefficients $\{u_p, v_p\}$ relate to $\{\eta_p\}$ through $\eta_p = v_p/u_p$. Clearly the BCS wavefunction is a linear combination of AGPs with all possible number of electron pairs (up to an inconsequential normalization factor). The AGP of N pairs, Eq. (4), corresponds to the projected BCS (PBCS) state with the correct particle number. The AGP ground state can be optimized on a classical computer at mean-field cost (see Sec. II B).

A. Beyond zero seniority

Seniority is defined as the number of unpaired electrons and is denoted by Ω [7]. Any two-body *ab initio* Hamiltonian can be written as [88]

$$H = H^{\delta\Omega=0} + H^{\delta\Omega=\pm 2} + H^{\delta\Omega=\pm 4}, \quad (9)$$

where the superscript differentiates between sectors of the Hamiltonian that change seniority by 0, ± 2 and ± 4 . The seniority-zero subspace features a remarkable simplicity [89–93], which makes it particularly convenient

for quantum algorithms [54, 94]. One can define a $su(2)$ pairing algebra with the generators

$$\mathbf{P}_p^\dagger = a_p^\dagger a_{\bar{p}}^\dagger, \quad (10a)$$

$$\mathbf{N}_p = a_p^\dagger a_p + a_{\bar{p}}^\dagger a_{\bar{p}}, \quad (10b)$$

and posit a *paired* encoding, $\mathbf{P}_p^\dagger \mapsto \frac{1}{2}(X_p - iY_p)$ and $\mathbf{N}_p \mapsto 1 - Z_p$, such that the qubit states $|1\rangle = \begin{pmatrix} 0 \\ 1 \end{pmatrix}$ and $|0\rangle = \begin{pmatrix} 1 \\ 0 \end{pmatrix}$ correspond to an electron-pair being present and absent respectively; here, X, Y , and Z are Pauli matrices. Any seniority-zero Hamiltonian can be encoded as

$$H^{\delta\Omega=0} \mapsto \sum_p h_p Z_p + \sum_{pq} w_{pq} Z_p Z_q + \sum_{pq} v_{pq} (X_p X_q + Y_p Y_q), \quad (11)$$

where w and v are Hermitian matrices. For most Hamiltonians, seniority is not a good quantum number, and the restriction to the seniority-zero subspace leads to approximate energies. Indeed, for *ab initio* Hamiltonians, doubly-occupied configuration interaction [95–97] (an exact diagonalization method in the seniority-zero subspace) is not sufficient to reach chemical accuracy. Therefore it becomes necessary to incorporate broken pair excitations.

To allow pairs to break, we first need to map individual spin-orbitals to qubits. Our goal is to follow our formalism for seniority-zero [54] closely to take advantage of its low asymptotic scaling and other desirable properties. We want to implement AGP, again, in its natural orbital basis where all electrons are paired. Broken-pair excitations then come from the correlator that couples the reference to all seniority sectors of the Hamiltonian.

We interlace the qubits associated with natural orbitals p and \bar{p} (i.e. logical qubits of p (\bar{p}) correspond to odd (even) physical qubits), and adopt the Jordan–Wigner (JW) encoding of fermions [98], so that $a_p \mapsto \frac{1}{2}(X_p + iY_p) Z_{\bar{p}-1} Z_{p-1} \cdots Z_{\bar{1}} Z_1$ and $a_{\bar{p}} \mapsto \frac{1}{2}(X_{\bar{p}} + iY_{\bar{p}}) Z_p Z_{\bar{p}-1} Z_{p-1} \cdots Z_{\bar{1}} Z_1$. Note that the paired encoding of Eq. (10) is embedded in this mapping. The BCS state can be implemented at $\mathcal{O}(1)$ depth with M two-qubit gates acting on every p, \bar{p} qubits [50, 54, 99],

$$|\text{BCS}\rangle = \prod_{p=1}^M e^{i\theta_p (X_{\bar{p}} X_p + Y_{\bar{p}} Y_p)/2} |\mathbf{0}\rangle, \quad (12)$$

where we have defined $\theta_p = 2 \arctan(\eta_p)$. If one chooses to obtain AGP from gauge integration,

$$|\text{AGP}\rangle = \frac{1}{2\pi} \int_0^{2\pi} d\phi e^{i\phi(\hat{N}-2N)} |\text{BCS}\rangle, \quad (13)$$

where $\hat{N} = \sum_p (a_p^\dagger a_p + a_{\bar{p}}^\dagger a_{\bar{p}})$, we can follow the procedure outlined in Ref. [54], whereby we introduce an ancilla qubit to compute grid-point overlaps $\langle \text{BCS} | \hat{\mathcal{O}}_{\mathcal{R}_i} | \text{BCS} \rangle$

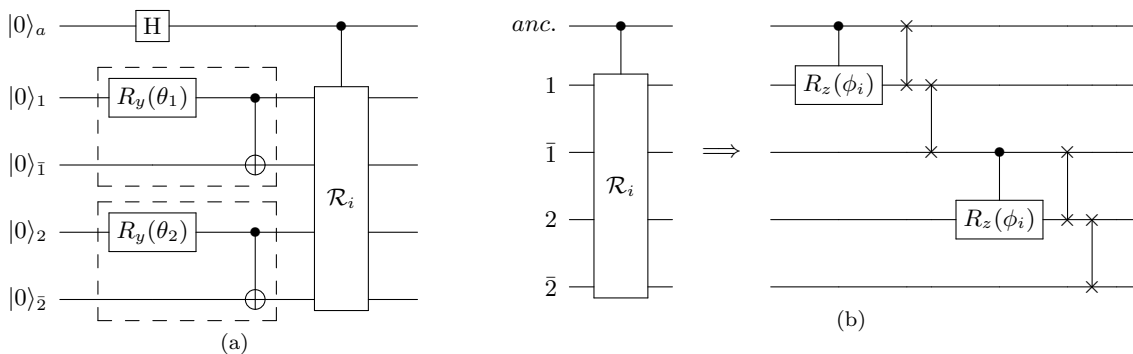


FIG. 1. Circuits to implement the number projected BCS wavefunction for seniority nonzero applications using the integral. Here it is shown for a system with 4 spin-orbitals ($M = 2$) for simplicity. (a) Implementation of the BCS wavefunction and circuit to do Hadamard test for every grid angle ϕ_i . The dashed box implements $\exp(i\theta_p(X_{\bar{p}}X_p + Y_{\bar{p}}Y_p)/2)$ acting on the vacuum state after simplification. (b) Implementation of the controlled $R_z(\phi_i)$ using nearest neighbors connectivity. Since the BCS orbitals p and \bar{p} are either simultaneously present or absent, the controlled $R_z(\phi_i)$ can be chosen to apply only to the “no-bar” qubits. The swap gates move the logical qubit of the ancilla qubit to the last qubit to measure $\langle X_a \rangle + i\langle Y_a \rangle$ needed for the Hadamard test.

via a Hadamard test, where \hat{O} is an arbitrary observable. For every gauge angle, ϕ_i , the operator \mathcal{R}_i takes the form

$$\mathcal{R}_i = e^{i\phi_i(\hat{N}-2N)} \mapsto e^{i\chi_i} \prod_{p=1}^M e^{-i\phi_i Z_p/2} e^{-i\phi_i Z_{\bar{p}}/2}, \quad (14)$$

where N is the number of pairs, and χ_i is a constant phase that can be incorporated on a classical computer. Further simplification is possible by noting that the state of qubit p must be identical to its conjugate pair \bar{p} in the BCS wavefunction. Thus, it suffices to construct \mathcal{R}_i such that it runs either on p or \bar{p} orbitals only. This simplification is only possible if the \mathcal{R}_i circuit is applied immediately after the BCS circuit. A circuit diagram combining the BCS implementation with number projection is depicted in Fig. (1) The depth of the circuit is $\mathcal{O}(M)$ and we need $\mathcal{O}(M)$ grid point to do the integration exactly. In Sec. III, we analyze an alternative to gauge integration by using post-selection.

B. AGP optimization

Our discussion so far has focused on how to implement AGP when $\{\eta_p\}$ and the pairing scheme are given; very little has been said on how they can be obtained. Recall that for a generic *ab initio* Hamiltonian,

$$H = \sum_{pq} h_{pq} c_p^\dagger c_q + \frac{1}{2} \sum_{pqrs} v_{pqrs} c_p^\dagger c_q^\dagger c_s c_r, \quad (15)$$

the AGP energy is not invariant under orbital rotation, so we need to optimize the geminal coefficients and the natural orbitals together. The latter determines the pairing scheme of the geminal. In what follows, we discuss two methods to optimize AGP for seniority nonzero Hamiltonians.

1. Direct optimization

We can always write down the Hamiltonian in the natural orbital basis as

$$e^{-\sigma} H e^{\sigma} = \sum_{pq} \tilde{h}_{pq}(D) a_p^\dagger a_q + \frac{1}{2} \sum_{pqrs} \tilde{v}_{pqrs}(D) a_p^\dagger a_q^\dagger a_s a_r, \quad (16)$$

where σ is the number-conserving Thouless operator defined as [100]

$$\sigma = \sum_{p>q} [\log(D)]_{pq} (c_p^\dagger c_q - c_q^\dagger c_p); \quad (17)$$

$\tilde{h}(D)$ and $\tilde{v}(D)$ are the one- and two-electron integrals transformed into the natural orbital basis. To obtain an optimized AGP, we need to variationally minimize the energy with respect to $\{\eta_p\}$ together with $\{D_{pq}\}$, where the overlaps are taken with respect the AGP state of the form Eq. (4) and Eq. (7). On a classical computer, all relevant reduced density matrices (RDMs) can be computed efficiently using the *sumESP* algorithm and the reconstruction formulas outlined in Ref. [54] or using generalized Wick’s theorem and one-body BCS transition RDMs [67, 101].

We may also opt for optimizing AGP on a quantum computer. This is useful, for example, when we perform reference optimization in the presence of the uCC correlator (see Sec. IV B). The unitary Thouless rotation, $\exp(\sigma)$, can be decomposed into a product of 2-qubit gates using the QR decomposition and Givens rotations [102], and so, it can be implemented exactly with linear circuit depth. This allows us to optimize the reference on a quantum computer without incurring any Trotterization error. All gradients with respect to $\{D_{pq}\}$ and $\{\eta_p\}$ can be computed efficiently by the fermionic shift-rule [103–105]. Note that the Hamiltonian is measured

in the atomic-orbital basis, Eq. (15), since the orbital rotation are absorbed into the circuit. Alternatively, it is also possible to work with Eq. (16), which is essentially the approach taken in Refs. [106, 107]. However, we adopt the former method in this work as it requires considerably fewer terms to measure.

In analogy with the HF wavefunction being classified by different spin-symmetry restrictions, i.e. restricted (RHF), unrestricted (UHF), and generalized (GHF) [3], we may choose to retain S^2 and/or S_z symmetries in AGP. These symmetries are reflected in the matrix elements of D , which we treat as independent variables during the optimization if we decide to allow the symmetries to break. Just as in HF theory, RAGP denotes spin-restricted AGP; UAGP denotes spin-unrestricted AGP (broken S^2); and GAGP denotes generalized AGP (broken S^2 and S_z).

2. Number projected Hartree–Fock–Bogoliubov

An alternative way to optimize AGP is through number projecting the Hartree–Fock–Bogoliubov (HFB) wavefunction. The equivalence between number-projected HFB (NHFB) and AGP with optimized natural orbitals is guaranteed by the Bloch–Messiah theorem [108], which states that the Bogoliubov quasiparticle operators defining an HFB state can be constructed from the physical fermionic operators through three consecutive Bogoliubov transformations of special forms: An orbital rotation, a BCS transformation, and a rotation amongst quasiparticles. They are represented by the D , (\bar{U}, \bar{V}) , and C transformations in Appendix A 1, respectively. The last C transformation is not physically significant since it only alters the global phase. Therefore, the broken-symmetry HFB state in an NHFB is essentially a BCS state with optimized orbitals, and variationally minimizing the PBCS or AGP energy with respect to both $\{D_{pq}\}$ and $\{\eta_p\}$ amounts to minimizing the NHFB energy in the variation-after-projection scheme [11, 109, 110].

An algorithm for computing the Bloch–Messiah decomposition is outlined in Appendix A 2. This algorithm is used in Sec. IV to prepare the initial UAGP references, where we extract the $\{D_{pq}\}$ and $\{\eta_p\}$ from the deformed HFB of the optimized number-projected spin-unrestricted HFB (NUHFB) wavefunction.

C. Disentangled uCC on AGP

Given an optimized AGP for an *ab initio* Hamiltonian, we define the singles and doubles anti-Hermitian coupled cluster operators [111, 112]

$$T_1 = \sum_{p>q} t_p^q (a_p^\dagger a_q - h.c.), \quad (18a)$$

$$T_2 = \sum_{pq>rs} t_{rs}^{pq} (a_p^\dagger a_q^\dagger a_s a_r - h.c.), \quad (18b)$$

where the indices run over spin-orbitals in the natural orbital basis. Higher order excitations can be defined similarly. Just as in HF theory, the uCC operators can be spin-restricted (uRCC), spin-unrestricted (uUCC), or spin-general (uGCC) [5]. For HF-based uCC, the cluster operators may be chosen over particles and holes only, or they can be general index, i.e. include hole-hole and particle-particle excitations [111]. In AGP, the separation between particles and holes is not well defined since the wavefunction inherently contains all possible ways N pairs occupy M orbitals [64]. Therefore the general correlator is most natural on AGP. (We shall return to defining particle–hole excitations on AGP later in Sec. IV B.)

On a quantum computer, uCC needs to be expressed in terms of elementary gates. We resort to using the disentangled uCC *Ansatz* [1, 19, 20], as in Eq. (1). Note that the disentangled uCC is number conserving throughout the implementation; for example, it is easy to verify that every term in

$$\begin{aligned} a_p^\dagger a_q^\dagger a_r a_s - h.c. \mapsto & \frac{-i}{8} \left(Y_p X_q X_r X_s + X_p Y_q X_r X_s \right. \\ & - X_p X_q Y_r X_s - X_p X_q X_r Y_s \\ & - X_p Y_q Y_r Y_s - Y_p X_q Y_r Y_s \\ & \left. + Y_p Y_q X_r Y_s + Y_p Y_q Y_r X_s \right) \prod_n Z_n, \quad (19) \end{aligned}$$

mutually commutes and together conserve particle number even after writing it as a product of exponentials. Computing the gradient on the hardware could follow Refs. [103–105]. Overall, the implementation cost and asymptotic scaling of uCC is the same as that of HF. Indeed, recent advancements in finding a lower-rank representation of an *Ansatz* or address the ordering ambiguity [19, 31, 113–118] are applicable to AGP-based calculations as well.

The Hamiltonian transformation can be done either using Eq. (16), or we can implement the Thouless rotations on the circuit and measure the Hamiltonian in the on-site or atomic orbital basis. The trade-off between the two approaches is well known [119–121]. Typically the Hamiltonian is sparser in the on-site basis, hence requiring fewer terms to measure; this comes at the expense of implementing the orbital rotation on a quantum computer, which is often less expensive than implementing uCC. Following the discussion in Sec. II B 1 and the method in Ref. [102], we can implement the orbital rotations with $\mathcal{O}(M)$ circuit depth with only nearest neighbors Givens rotations appended to the end of the *Ansatz* circuit.

III. POST-SELECTION

Computing the expectation value of an observable \hat{O} with respect to a wavefunction $|\psi\rangle$ on a quantum computer entails rotating \hat{O} to the computational basis by some unitary operator \hat{V} (i.e. $\hat{O} = \hat{V}^\dagger \hat{\Lambda} \hat{V}$), and empirically estimating $\sum_a \lambda_a |\langle \lambda_a | \hat{V} | \psi \rangle|^2$, where λ_a is an eigen-

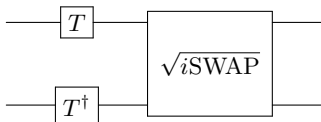


FIG. 2. Number conserving circuit that diagonalizes $X_p X_q + Y_p Y_q$ [123]. The T-gate is $R_z(\pi/4)$.

value of $\hat{\Lambda}$ [122]. Often, diagonalizing \hat{O} could be expensive or even prohibitive, but if \hat{O} is expressible as a linear combination of Pauli matrices (e.g. *ab initio* Hamiltonians under the JW transformation), we can sample the Pauli terms separately where the diagonalization is often straightforward.

Now suppose \hat{O} commutes with some symmetry operator \hat{S} . We want to measure \hat{O} along with its symmetry eigenvalues in order to project out samples that belong to the undesired symmetry sectors. To do this, we need to diagonalize \hat{O} in its shared eigenbasis with \hat{S} . This involves finding disjoint sets of Pauli matrices of \hat{O} that commute amongst each other as well as with \hat{S} , then diagonalize and measure each group separately. As an example, consider measuring the energy of a general seniority-zero Hamiltonian, Eq. (11), and suppose we want to post-select based on the particle number symmetry i.e. $\hat{S} = \sum_p \mathbf{N}_p$. The first two terms, $\sum_p h_p Z_p + \sum_{pq} v_{pq} Z_p Z_q$, are readily in the computational basis and conserve particle number; for the last term, one needs to diagonalize $X_p X_q + Y_p Y_q$ with a number conserving unitary, \hat{V} , to get [123]

$$\frac{1}{2} \langle X_p X_q + Y_p Y_q \rangle = \frac{1}{2} \langle \hat{V}^\dagger (Z_q - Z_p) \hat{V} \rangle. \quad (20)$$

See Fig. (2). Computing RDMs in seniority nonzero systems follows the same idea and involves grouping Pauli terms into fragments of mutually commuting and number conserving terms. Indeed, some of the most efficient strategies to find optimal fragments that minimize the scaling of the total number of measurements in VQE, such as the “basis rotation grouping” of Ref. [86] and the “full rank optimization” and its variants of Ref. [124], create fragments that conserve particle number by construction. Thus, we can readily adopt these strategies for AGP post-selection, thereby alleviating concerns about the significant overhead needed to obtain number conserving subsets.

Post-selection has gained attention as a useful method to mitigate noise when sampling from quantum hardware [82–84, 86, 123, 125–127]. However, our goal in this section is to use post-selection as an alternative to gauge integration to restore particle number and sample over the correlated AGP wavefunction. We present an analysis of the cost and scaling of post-selection and show how to adjust $\{\eta_p\}$ to maximize getting samples in the desired particle sector. It is noteworthy that post-selection and the gauge integration are not necessarily mutually exclusive; to restore multiple symmetries, one might choose

to use a combination of the integral and post-selection, should that provide an advantage. In this paper, we concentrate on restoring number symmetry only and leave the analysis of other symmetries for future work.

We must mention that there are alternative ways to observing symmetries prior to the final measurement, such as phase estimation on \hat{S} or other circuits [18, 50, 51, 53, 83, 125]. In these methods, typically a specialized circuit is applied in the *bulk* of the circuit and symmetries are observed with the help of ancilla qubits. Our strategy to maximize sample outcomes and scaling analysis of the number of measurements applies to those methods as well.

A. Procedure

To compute expectation values over AGP, we need to implement the corresponding BCS wavefunction, correlated it, and perform post-selection at the end. To this end, it is crucial that we use a number conserving correlator, since

$$\hat{U}|\text{AGP}\rangle = \hat{U}(\mathcal{P}_N|\text{BCS}\rangle) = \mathcal{P}_N \hat{U}|\text{BCS}\rangle, \quad (21)$$

is true if and only if $[\mathcal{P}_N, \hat{U}] = 0$, where \hat{U} is the correlator and \mathcal{P}_N is the number projection operator. The disentangled uCC as described in Sec. II C satisfies this requirement.

In general, however, $\langle \text{BCS} | \hat{N} | \text{BCS} \rangle \neq 2N$, due to the broken $U(1)$ gauge degree of freedom in the BCS wavefunction [7]. This could lead to nonoptimal sampling during post-selection since we get samples that do not belong to the desired particle number sector on average. Fortunately, we can fix the gauge to $\langle \hat{N} \rangle = 2N$ easily during the AGP optimization using projected BCS or NHFB by introducing a chemical potential. Doing so amounts to multiplying all η_p by a constant number which does not change expectation values over AGP [64]. Alternatively we can find this constant algebraically. See Appendix B 1.

A major advantage of using post-selection compared to gauge integration over the same Pauli set is the lack of an additional ancilla qubit needed to perform the Hadamard test, and the $\mathcal{O}(M)$ circuit depth for the controlled $R_z(\phi_i)$ rotations. However, the difference in the scaling of number of measurements is more involved. For the integral, the number of measurements scales as $\mathcal{O}(M)$ corresponding to the total number of grid points, and it is independent of the Hamiltonian. To derive the scaling for post-selection, we formulate the problem as follows: *What is the minimum number of measurements needed to get at least one observation in the correct number sector with $\alpha \times 100$ percent confidence?* We show in Appendix B 2 that the number of measurements, n , is given by

$$n = \left\lceil \frac{\log(1 - \alpha)}{\log(1 - P)} \right\rceil, \quad (22)$$

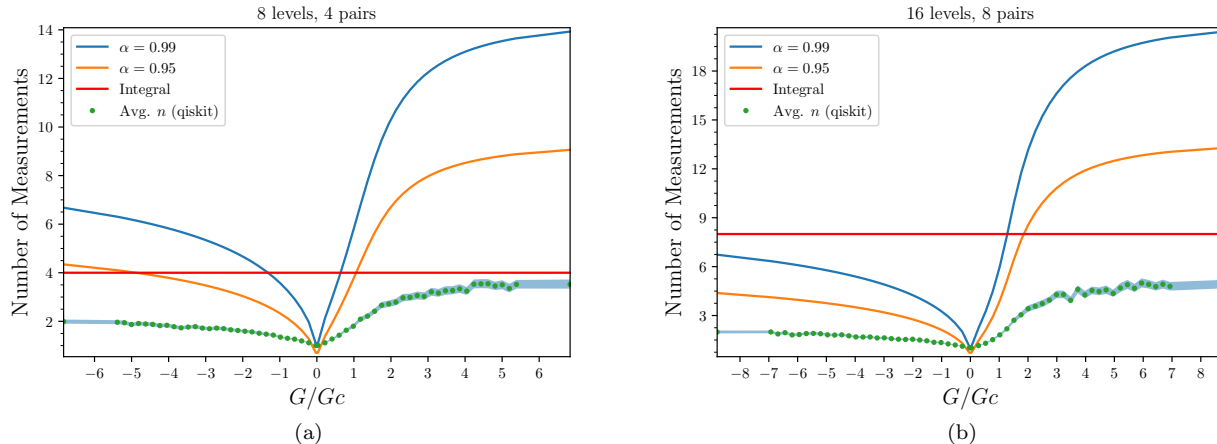


FIG. 3. Estimated number of measurements, n , needed to get at least one observation with the correct particle number as a function of G/G_c for the pairing Hamiltonian with 8 (a) and 16 (b) orbitals at half-filling. The red curve corresponds to the number of grid points to carry out number projection with gauge integration. The green dots are the average number for n obtained experimentally from 10^3 parallel runs on a noise-less quantum simulator (`qiskit`) along with their 95% confidence intervals (shaded area). The blue and orange curves are theoretical upper bounds for n with $\alpha = 0.95, 0.99$ computed from Eq. (22).

where $P = (\prod_p u_p^2) S_N^M$, and S_N^M is an elementary symmetric polynomial associated with the norm of AGP [64]. Clearly n depends on the details of the Hamiltonian through P , which itself is a function of $\{\eta_p\}$. The largest value of n occurs when number symmetry is strongly broken and all $\{\eta_p\}$ approach the same value. This is the worst case scenario for post-selection and, as we show in Appendix B 2, it is asymptotically bounded above by $\mathcal{O}(\sqrt{M})$. In regimes where number symmetry does not break, the scaling could be as low as $\mathcal{O}(1)$.

B. Numerical experiments

We put the scaling to numerical test by doing post-selection for the pairing Hamiltonian [7, 128],

$$H = \sum_p \epsilon_p \mathbf{N}_p - G \sum_{pq} \mathbf{P}_p^\dagger \mathbf{P}_q, \quad (23)$$

written here in the pairing algebra; $\epsilon_p = p\Delta\epsilon$ are the single particle energy levels and G tunes the strength of the pair-wise interaction and has infinite range. The pairing model is an ideal benchmark as the mean-field breaks number symmetry—gives rise to a BCS state—at $G = G_c > 0$ where number fluctuations get larger as G increases; for all $G < G_c$ (including $G < 0$) the mean-field admits a single HF Slater determinant for which the corresponding particle number fluctuations are small.

In Fig. (3) we plot n computed from Eq. (22) with $\alpha = 0.95$ and 0.99 as a function of G/G_c for 8 and 16 orbitals at half-filling. Half-filling is the ideal case for the integration as it requires the fewest number of grid points, whereas the opposite is true for post-selection.

We also numerically simulated post-selection on `qiskit` [129], using the QASM simulation libraries in the absence of noise. For every G point, we simulated the BCS state and performed multiple measurements until we got an outcome with the correct particle number. This process was repeated 10^3 to estimate n by the empirical mean, \bar{n} . The 95% confidence intervals were computed from bootstrapping the samples 10^4 times and are shown with the shaded area in the plot. As we can see, the sample means along with their confidence intervals are below the number of measurements needed for the integral for all points, even in $G \gg G_c$ where number fluctuations are large. This suggests that number symmetry restoration with post-selection could be a viable alternative to gauge integration even in small systems with large number fluctuations.

In Fig. (4) we numerically investigate the scaling of post-selection as a function of system size M . On the left hand side of Fig. (4) we plot the sample means, \bar{n} , computed at different G/G_c points on a log-log scale as a function of the system size M . Linear fits to the mean resulted in slopes: $m = 0.449, 0.488, 0.392, -0.01, 0.027, -0.02$ rounded to the closest digits in decreasing order of G . On the right side of the figure, we used Eq. (22) to compute n beyond what we could simulate on `qiskit`, with system size as large as $M = 40$. The results suggest $\mathcal{O}(1)$ scaling in $G < 0$, where number symmetry does not break, and a $\mathcal{O}(\sqrt{M})$ where number symmetry breaks. This is inline with the $\mathcal{O}(\sqrt{M})$ asymptotic scaling found analytically and shown in detail in Appendix B 2.

In summary, Table I compares the scaling cost of phase estimation, exact gauge integration, and post-selection as

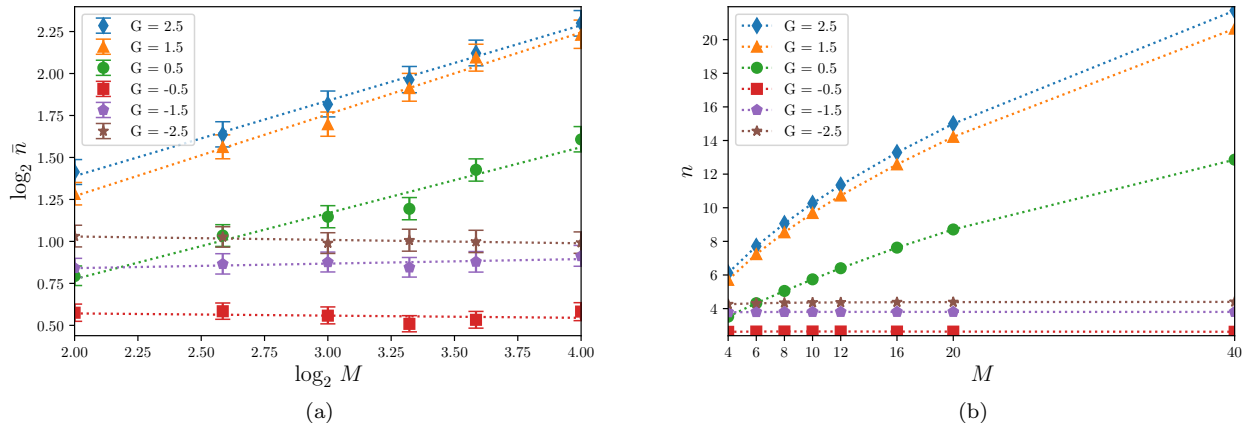


FIG. 4. Scaling of post-selection as function of system size, M , for the pairing Hamiltonian. (a) The average number of measurements, \bar{n} , to get one observation with the correct particle number from repeated sampling on a quantum emulator (`qiskit`). The error bars correspond to the 95% confidence intervals. This was performed for $M = 4, 6, 8, 10, 12, 16$ at different G values. (b) The theoretical number of measurements on a linear scale computed from Eq. (22) with $\alpha = 0.95$. This allows us to estimate n for system much larger than those we can simulate on `qiskit`.

methods to restore number symmetry. For phase estimation, one could follow Refs. [50, 125] and use our technique to guarantee an $\mathcal{O}(\sqrt{M})$ scaling for the number of measurements. If mid-circuit measurement is feasible on a quantum computer, then phase estimation can be carried out with only one ancilla qubit i.e. $\mathcal{O}(1)$ scaling instead of $\mathcal{O}(\log(M))$.

IV. APPLICATION

Having developed a method for how to optimize and implement AGP for quantum computers, we concentrate on building correlation atop of AGP for seniority nonzero applications in this section. Our aim is to showcase our method by benchmarking it against the ground state of the single-band Fermi–Hubbard model,

$$H = -t \sum_{\langle p,q \rangle} \sum_{\sigma \in \{\uparrow, \downarrow\}} (c_{p\sigma}^\dagger c_{q\sigma} + h.c.) + U \sum_p n_{p\uparrow} n_{p\downarrow}, \quad (24)$$

written here in its on-site basis, where $n_{p\sigma} = c_{p\sigma}^\dagger c_{p\sigma}$. We set $t = 1$ for simplicity for the rest of this section.

Method	Measurements	Depth	Ancilla qubits
Phase estimation	$\mathcal{O}(\sqrt{M})$	$\mathcal{O}(M \log(M))$	$\mathcal{O}(\log(M))$
Gauge integral	$\mathcal{O}(M)$	$\mathcal{O}(M)$	$\mathcal{O}(1)$
Post-selection	$\mathcal{O}(\sqrt{M})$	$\mathcal{O}(1)$	None

TABLE I. Scaling of number symmetry restoration using different methods as a function of system size (M) for a given number-conserving Pauli fragment.

For this Hamiltonian, number symmetry breaks at some finite $U < 0$ value; and when $U > 0$, the mean-field breaks spin-symmetry at a critical $U > 0$. While one of the main advantages of using AGP is for models wherein the two-body interactions are attractive, we showcase our method in both the repulsive and attractive regimes of this Hamiltonian. Our strategy is to allow the S^2 symmetry to break (i.e. use UAGP) and correlate the resulting wavefunction. This helps us illustrate the utility of AGP in all regimes—attractive, repulsive, weak and strong limits. Indeed, to improve the results even more, one can envision restoring S_z and/or S^2 which tend to break at sufficient strong correlation, but we leave those for future work.

We first present the results for the fixed-reference methods, wherein we have optimized UAGP on a classical computer and use quantum computers to optimize uCC atop of AGP. In the later half of this section, we demonstrate another powerful *Ansatz* based on a particle–hole unitary, which as we shall see, needs to be optimized simultaneously with the reference AGP.

The Implementation details of this section can be found in Appendix C.

A. Fixed-reference

We implement our *Ansätze* with the following structure,

$$|\psi\rangle = \underbrace{\prod_k e^{\sigma_k}}_{\text{orbital rotation}} \underbrace{\left(\prod_d e^{\hat{D}_d} \right)}_{\text{doubles}} \underbrace{\left(\prod_s e^{\hat{S}_s} \right)}_{\text{singles}} |\phi\rangle, \quad (25)$$

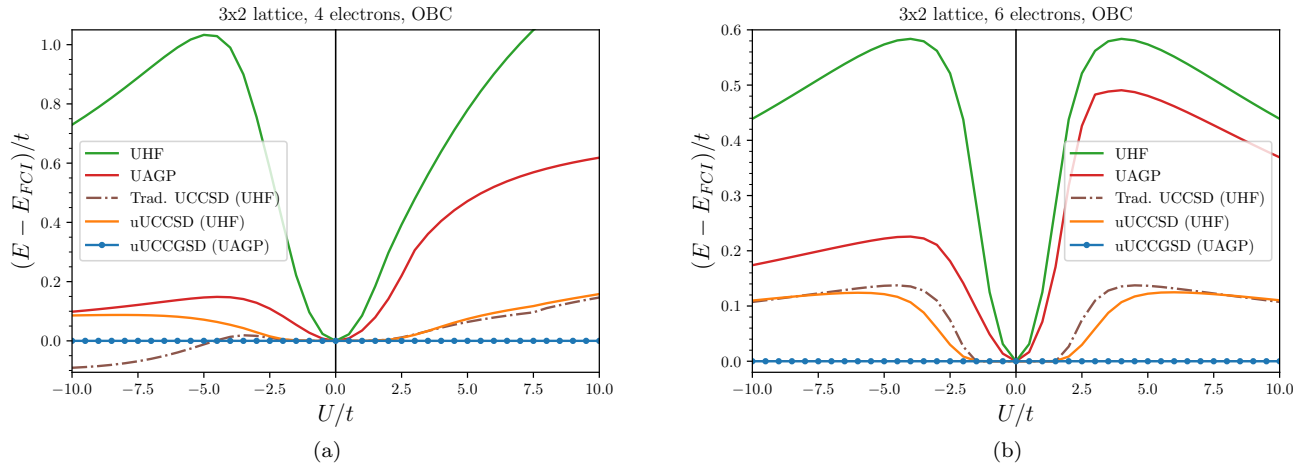


FIG. 5. Energy error of fixed-reference calculations for 2D Hubbard with open boundary conditions (OBC) away from half-filling (a) and at half-filling (b) as a function of U/t . Traditional (Trad.) or disentangled unitary (u) spin-unrestricted coupled cluster calculations were performed based on UHF or UAGP references with single and double excitations (UCCSD) or their generalized coupled cluster counterpart (UCCGSD).

where $|\phi\rangle$ can be AGP or HF. The orbital rotation is optional but it allows one to measure the Hamiltonian in the on-site basis which is significantly sparser and simpler than the natural orbital basis (see Sec. II C). The on-site Hubbard Hamiltonian is also convenient for post-selection as it maps to

$$H = \frac{t}{2} \sum_{\langle p,q \rangle} \sum_{\sigma \in \{\uparrow, \downarrow\}} (X_{p\sigma} X_{q\sigma} + Y_{p\sigma} Y_{q\sigma}) \prod_n Z_n + \frac{U}{4} \sum_p (1 - Z_{p\uparrow})(1 - Z_{p\downarrow}), \quad (26)$$

under the JW transformation. The only fragment that needs to be diagonalized is the nearest-neighbors hopping terms, for which we can apply the same circuit as the seniority-zero Hamiltonians shown in Fig. (2).

In Fig. (5) we show the VQE calculation results for the 2D Hubbard model at half-filling and away from half-filling with open boundary conditions (OBC). For the doped system, the number symmetry becomes strongly broken as $U < 0$ get smaller. This is the kind of regime where we expect AGP-based methods to excel and traditional methods to struggle. Indeed, traditional UCCSD over-correlates in the 4-electron case as U gets smaller and becomes difficult to converge starting near $U \approx -8$ up to some finite regime of U . In the $U > 0$ regime of the same doped system, in addition to S^2 , S_z symmetry breaks at mean-field near $U \sim 7.5$; only the S^2 symmetry breaks for the half-filled case.

We plot uUCCGSD based on UAGP for all values of U . As a point of reference, we have plotted uUCCSD on UHF as well. The AGP-based results captured energies with absolute errors as small as 10^{-9} for both systems which is where we set the tolerance of our optimization.

While this confirms that our AGP-based method is capable of accessing all relevant parts of the Hilbert space (not just seniority-zero for example) and get almost exact energies for these system, the high accuracy might be in part due its high number of variational parameters compared to the dimension of FCI. There are 870 variational parameters in uUCCGSD while the FCI dimension of the half-filled and doped systems are $\binom{12}{6} = 924$ and $\binom{12}{4} = 495$ respectively. We get equally good results with uUCCGSD on UHF for these systems. While this in principle can be tested by going to larger systems, our current implementation of the code allows for maximum system size of 12 spin-orbitals.

To find a sparser representation of the disentangled uUCCGSD we performed ADAPT-VQE [25] calculations with the same operator pool as uUCCGSD for the 4-electron system. ADAPT-VQE was designed and tested for HF-based methods, but we follow the same idea for our implementation and use AGP as our reference. We set ADAPT's stopping criterion to be $\epsilon = 10^{-3}$. As shown in Fig. (6) energy errors of 10^{-6} were obtained with as few as 60 parameters with AGP. For comparison we also plotted particle-hole and general index HF-based calculations with the same computational settings. We observe the largest gains with AGP-based ADAPT in the regimes where number symmetry breaks and the system is strongly correlated. In large $U > 0$, we did not see significant advantage in using AGP compared with HF. More studies are needed to tailor ADAPT for AGP-based methods. After submitting this paper, the recent work by Refs. [130, 131] has come to our attention in which the authors studied the affect of symmetry breaking in the ADAPT-VQE framework. While neither investigated the restoration of particle number symmetry, our results with AGP is complementary to their findings in that restoring

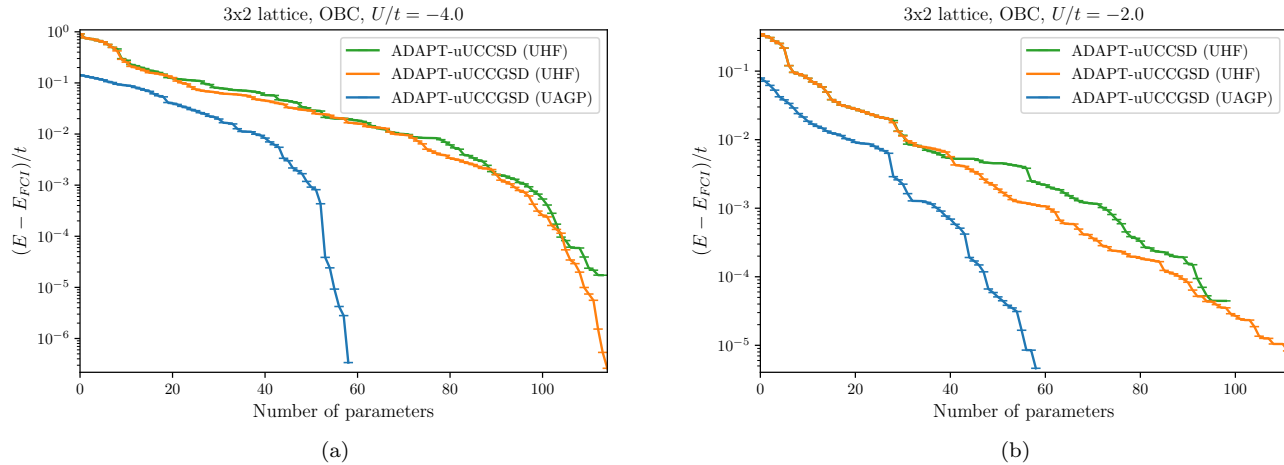


FIG. 6. ADAPT-VQE calculations for HF- and AGP-based disentangled uCC (fixed-reference) for the 4 electron system at the strongly correlated point ($U/t = -4$) where mean-field methods struggle the most and a slightly less correlated point ($U/t = -2$) for comparison.

symmetries that spontaneously break at the mean-field level could greatly benefit ADAPT’s convergence.

In the next section, we develop a particle–hole *Ansatz* on AGP which has considerably fewer parameters than uUCCGSD.

B. Reference-optimized uCC

One of the main advantages of using the uCC *Ansatz* with particle–hole excitations is that it is significantly more concise compared to one based on general operators. Ideally, we would like to develop a particle–hole uCC *Ansatz* based on AGP.

In general, the natural orbitals of AGP and HF are different. In the weakly correlated limit (e.g. $U \rightarrow 0$ for the Hubbard Hamiltonian), the HF and AGP orbitals converge to the same values and we get $\eta_1, \dots, \eta_N \rightarrow 1$ and $\eta_{N+1}, \dots, \eta_M \rightarrow 0$ (up to a global const) so that AGP becomes just a single Slater determinant [65]. For finite, nonzero U , we designate the first N orbitals of the largest occupations as *occupied* and the rest *virtual*, thereby defining a “particle–hole” picture from which we can define our cluster operators. In our numerical experiments, particle–hole disentangled uCC makes only a small improvement on mean-field AGP in the attractive regime. However, we can remedy this by optimizing the AGP orbitals and geminal coefficients in the presence of the particle–hole correlator. As we shall see, we obtain significant improvement by so doing. Our observation is consistent with the results obtained in Ref. [132] which was carried out for the pairing Hamiltonian.

Again, we implemented Eq. (25) for all of our *Ansatz*. However, instead of fixed orbital-rotation parameters, we optimized them simultaneously with uCC amplitudes. For AGP-based methods, we also optimized $\{\eta_p\}$ as dis-

cussed in Sec. II B. Indeed, for HF, reference optimization corresponds to optimizing the orbitals only. For all cases, the Hamiltonian was measured in the on-site basis.

In Fig. (7) we show the results for the particle–hole uCC based on UAGP for 6 sites, 1- and 2-dimensions, with 4 and 6 electrons. We performed UHF-based calculations with the same optimization settings and *Ansatz* ordering as those for AGP. Just as in the fixed-reference case, we observed largest gains in the attractive regime. Nevertheless, our numerical results suggest that AGP can be just as competitive as HF in $U > 0$ as a starting point for corrected method in all of the systems that we tried.

V. DISCUSSIONS

A desirable property for electronic structure methods is accurately describing the weakly and strongly correlated regimes seamlessly. One way to achieve this goal is to restore symmetries that break at the mean-field level as the result of strong correlation and capture the remaining correlation energy using CC-type correlators.

Building on our previous work that dealt with correlating AGP in the seniority-zero subspace, we developed a coupled cluster method to correlate AGP for general, seniority nonzero Hamiltonians on a quantum computer. We benchmarked our numerical results against the ground state of the Fermi–Hubbard Hamiltonian—a model Hamiltonian that breaks number symmetry when $U < 0$ and breaks various spin-symmetries when $U > 0$.

We proposed two techniques: First, we optimize AGP on a classical computer then correlate it on a quantum computer. We showed that uUCCGSD on AGP is highly accurate and capable of accessing all relevant parts of the Hilbert space. Using a naïve implementation of ADAPT-

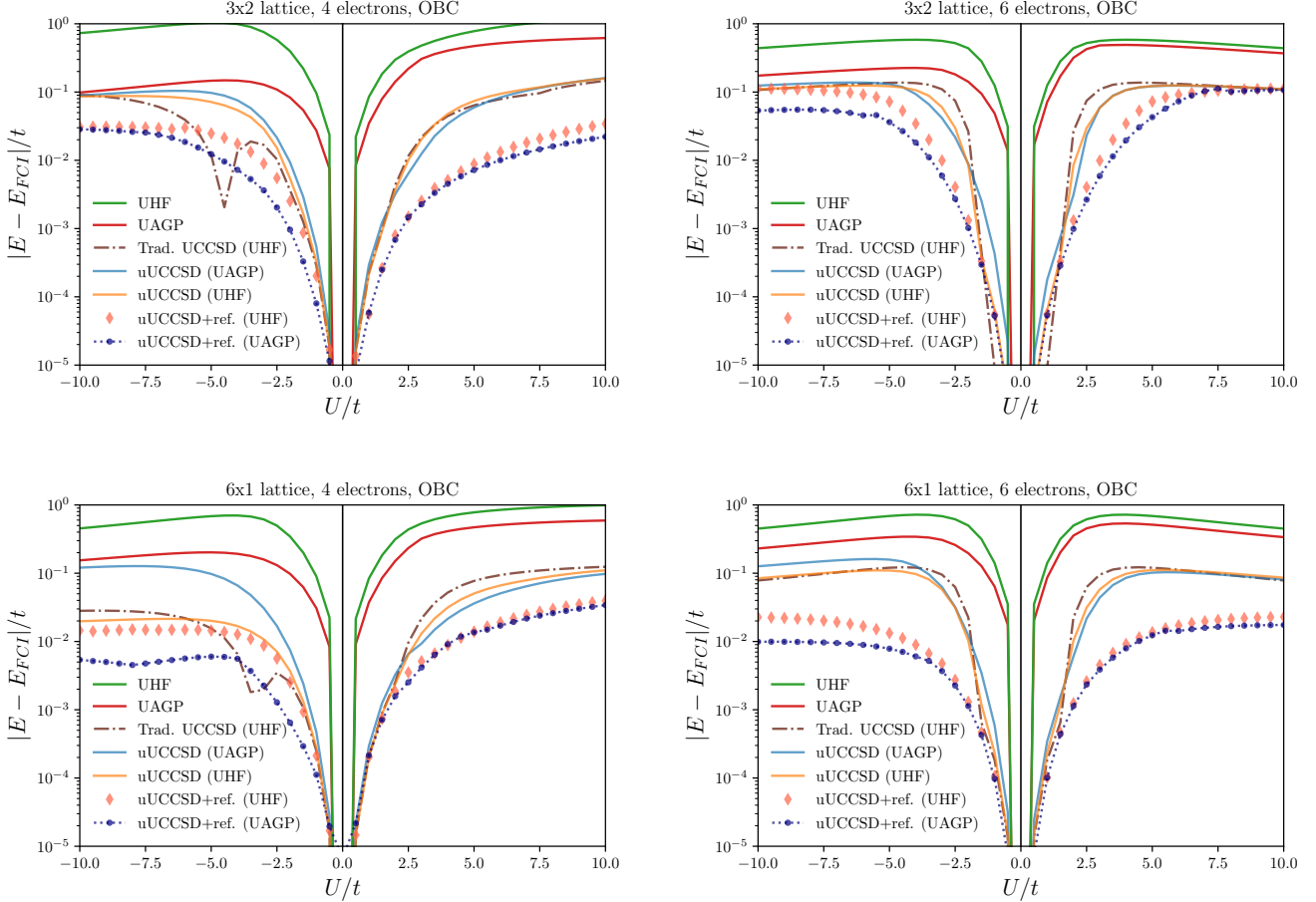


FIG. 7. A particle–hole uCC *Ansatz* based on UAGP and UHF tested for one and two dimensional Hubbard model at and away from half-filling. Methods involving reference optimization are denoted by “+ref.”

VQE on AGP in a 2-dimensional, doped Hubbard model, we observed that AGP-based uUCCGSD could give a sparser, yet highly accurate *Ansatz* in the regime where number symmetry breaks. Our second technique uses a particle–hole uCC based on AGP. The separation between particles and holes in AGP is not as well-defined as HF, and the orbitals are generally very different. However, by relaxing the reference in the presence of the particle–hole uCC correlator, we obtained excellent results in our numerical benchmarks.

In addition to correlating AGP, we illustrated how post-selection can fit well into our formalism to restore particle number. Symmetry restoration can be realized in a variety of ways on a quantum computer, including gauge integration and phase estimation. Post-selection relieves the need for implementing the Hadamard tests to evaluate the integral and is less expensive than phase estimation. Our main contribution is to show that the number of measurements in post-selection scales as $\mathcal{O}(\sqrt{M})$ in the worst case (where number is strongly-broken) in the absence of noise. We proved this analytically, and tested it numerically for the pairing Hamiltonian using a

quantum emulator. Our numerical results suggest scaling of as low as $\mathcal{O}(1)$ in the regime where number symmetry does not break. In contrast, the measurement cost of exact gauge integration is $\mathcal{O}(M)$ and independent of the strength of the correlation.

Post-selection on particle number is often a necessary step for noise mitigation on NISQ hardware. However, when performed on an *Ansatz* that deliberately breaks number symmetry, one can recover additional correlation energy, even in the regimes that number symmetry does not break. This observation together with the fact that the cost of constructing disentangled uCC on AGP is the same as HF on a quantum computer, could make AGP an attractive wavefunction for the strong correlation. Future work could benefit from restoring spin-symmetries, such as S^2 and S_z to further improve the accuracy of AGP-based methods for molecules. While issues related to the barren plateau problem [133] are less prominent for physically inspired *Ansätze*, future work could also explore convergence properties of AGP-based uCC.

VI. ACKNOWLEDGMENTS

This work was supported by the U.S. Department of Energy under Award No. DE-SC0019374. G.E.S. is a Welch Foundation Chair (C-0036). A.K. is thankful to Garnet Kin-Lic Chan for insightful consultations on post-selection and thanks Jonathon P. Misiewicz and Nicholas H. Stair for helpful inputs regarding QForté. G.P.C thanks Carlos A. Jimenez-Hoyos for discussions regarding NHFB and its implementation. A.K. and G.P.C are grateful to Thomas M. Henderson for helpful discussions.

APPENDIX

Appendix A: Bloch–Messiah decomposition

An HFB state is defined as the vacuum of Bogoliubov quasiparticles,

$$|\text{HFB}\rangle = \prod_{p=1}^{2M} \beta_p |\text{vac}\rangle, \quad (\text{A1})$$

where the *quasiparticle operators* β_p, β_p^\dagger are defined by a unitary canonical transformation \mathcal{W} of the physical fermionic operators c_p, c_p^\dagger ,

$$\begin{pmatrix} \beta \\ \beta^\dagger \end{pmatrix} = \mathcal{W}^\dagger \begin{pmatrix} c \\ c^\dagger \end{pmatrix} = \begin{pmatrix} U^\dagger & V^\dagger \\ V^T & U^T \end{pmatrix} \begin{pmatrix} c \\ c^\dagger \end{pmatrix}, \quad (\text{A2})$$

wherein U and V are known as the Bogoliubov coefficients. By the Bloch–Messiah decomposition, we can bring U and V into a canonical form, which enables us to write the HFB as a BCS wavefunction in the natural orbital basis. As a consequence, a NHFB state optimized on a classical computer can be used to prepare an AGP on a quantum computer.

1. Bloch–Messiah theorem

The Bloch–Messiah theorem states that \mathcal{W} can be decomposed into three unitary canonical transformations of special forms,

$$\mathcal{W} = \begin{pmatrix} U & V^* \\ V & U^* \end{pmatrix} = \begin{pmatrix} D & 0 \\ 0 & D^* \end{pmatrix} \begin{pmatrix} \bar{U} & \bar{V} \\ \bar{V} & \bar{U} \end{pmatrix} \begin{pmatrix} C & 0 \\ 0 & C^* \end{pmatrix}, \quad (\text{A3})$$

where D and C are unitary matrices and

$$\bar{U} = \bigoplus_{p=1}^M \begin{pmatrix} u_p & 0 \\ 0 & u_p \end{pmatrix}, \quad (\text{A4a})$$

$$\bar{V} = \bigoplus_{p=1}^M \begin{pmatrix} 0 & v_p \\ -v_p & 0 \end{pmatrix}, \quad (\text{A4b})$$

are real matrices whose nonzero elements are BCS coefficients $\{u_p, v_p\}$. D is called the canonical orbital coefficients and is identical to the natural orbital coefficients of the geminal defined in Eq. (6), hence the same symbol. This can be readily seen by recognizing $\eta = (VU^{-1})^*$ and $\bar{\eta} = (\bar{V}\bar{U}^{-1})^*$. Incidentally, the most general form of the Bloch–Messiah theorem applies to both odd and even electron systems, albeit we restrict ourselves to even electron systems herein.

2. Computing Bloch–Messiah decomposition

Given an HFB, we denote its one-particle reduce density matrix by ρ and pairing matrix by κ . ρ is Hermitian and κ antisymmetric. They relate to the Bogoliubov coefficients through [7]

$$\rho = V^* V^T, \quad (\text{A5a})$$

$$\kappa = V^* U^T, \quad (\text{A5b})$$

and thus satisfy

$$\rho \kappa = \kappa \rho^*, \quad (\text{A6a})$$

$$\rho - \rho^2 = \kappa \kappa^\dagger. \quad (\text{A6b})$$

Computing the Bloch–Messiah decomposition amounts to simultaneously diagonalizing ρ and canonicalizing κ [87] in the sense of

$$\bar{\rho} = \bigoplus_{p=1}^M \begin{pmatrix} \rho_p & 0 \\ 0 & \rho_p \end{pmatrix} = D^\dagger \rho D, \quad (\text{A7a})$$

$$\bar{\kappa} = \bigoplus_{p=1}^M \begin{pmatrix} 0 & \kappa_p \\ -\kappa_p & 0 \end{pmatrix} = D^\dagger \kappa D^*, \quad (\text{A7b})$$

where $\bar{\rho}$ and $\bar{\kappa}$ are real. To do this, we just need to canonicalize κ in each degenerate eigen subspace of ρ . Canonicalization of an antisymmetric matrix can be performed using algorithms described in [134]. Subsequently, $\{u_p, v_p\}$, or equivalently $\{\eta_p\}$, can be determined from the values of $\{\rho_p, \kappa_p\}$.

Specifically for UHFB, ρ and κ have the following spin block structures:

$$\rho = \begin{pmatrix} \rho^{\alpha\alpha} & 0 \\ 0 & \rho^{\beta\beta} \end{pmatrix}, \quad (\text{A8a})$$

$$\kappa = \begin{pmatrix} 0 & \kappa^{\alpha\beta} \\ -(\kappa^{\alpha\beta})^T & 0 \end{pmatrix}. \quad (\text{A8b})$$

By Eq. (A6), we have

$$\left[\rho^{\alpha\alpha}, \kappa^{\alpha\beta} (\kappa^{\alpha\beta})^\dagger \right] = 0, \quad (\text{A9a})$$

$$\left[\rho^{\beta\beta}, (\kappa^{\alpha\beta})^T \kappa^{\alpha\beta*} \right] = 0, \quad (\text{A9b})$$

which implies that we can simultaneously diagonalize the Hermitian matrices $\rho^{\alpha\alpha}$, $\rho^{\beta\beta}$, and $\kappa^{\alpha\beta}$ ($\kappa^{\alpha\beta}$)[†]. We can show that the eigenvalues of $\rho^{\alpha\alpha}$ are identical to those of $\rho^{\beta\beta}$. Moreover, we can always find unitary matrices D^α and D^β such that the columns of D^α are the eigenvectors of $\rho^{\alpha\alpha}$ and the left singular vectors of $\kappa^{\alpha\beta}$, while the columns of D^β are the eigenvectors of $\rho^{\beta\beta}$ and the complex conjugate of the right singular vectors of $\kappa^{\alpha\beta}$. The matrix of canonical orbital coefficients is then written as

$$D = \begin{pmatrix} D^\alpha & 0 \\ 0 & D^\beta \end{pmatrix} P^T, \quad (\text{A10})$$

where P is the permutation matrix of

$$\begin{pmatrix} 1 & 2 & \cdots & M & M+1 & M+2 & \cdots & 2M \\ 1 & 3 & \cdots & 2M-1 & 2 & 4 & \cdots & 2M \end{pmatrix}. \quad (\text{A11})$$

This permutation arises because we choose to put the paired spin-orbitals p and \bar{p} adjacent to each other in Eq. (A4). We see from Eq. (A10) that a (p, \bar{p}) pair in UHFB is a spin pair. Consequently, the natural orbital pairs in UAGP are spin pairs.

We can carry out a similar procedure to find the canonical orbital coefficients D and thereby the Bloch–Messiah decomposition for RHF. In this case, D is in the form of Eq. (A10) with $D^\alpha = D^\beta$.

Appendix B: Post-selection analysis

1. Fixing the gauge

As evident from Eq. (4), multiplying all $\{\eta_p\}$ by a constant, c , amounts to multiplying AGP by an inconsequential global constant c^N . The same however is not true for the BCS wavefunction, since a global constant cannot be factorized. In BCS, multiplying all η_p changes the average particle number. Therefore, given a set of η_p , we can solve for c so that the average particle number is fixed. Recall that,

$$\langle \text{BCS} | \hat{N} | \text{BCS} \rangle = \sum_{p=1}^M 2v_p^2 = 2 \sum_{p=1}^M \frac{\eta_p^2}{1 + \eta_p^2}, \quad (\text{B1})$$

where we used the fact that $\eta_p = v_p/u_p$ and $u_p^2 + v_p^2 = 1$ in the last equality. We need, $\langle \hat{N} \rangle = 2N$, so we can solve for c (it can be taken to be real) that satisfies,

$$\sum_p \frac{(c\eta_p)^2}{1 + (c\eta_p)^2} - N = 0. \quad (\text{B2})$$

We are not aware of a simple closed-form solution. However, it is easy to solve for c numerically with standard root finding algorithms. This can be particularly helpful when optimizing the reference AGP on a quantum computer such as Sec. IV B or Sec. II B, where for every guess of $\{\eta_p\}$, they can be scaled to maximize sampling outcomes.

2. Scaling of post-selection

We want show that the asymptotic scaling of post-selection is no worse than $\mathcal{O}(\sqrt{M})$. To this end, we first derive an analytical expression for the number of measurements needed to obtain at least one sample in the correct particle number sector. We then find an upper bound to this expression which gives us the asymptotic scaling.

Typically, we are interested in computing the expectation value of some observable \hat{O} over correlated AGP. we concentrate on number conserving operators, since otherwise their expectation values over AGP are zero. Let \hat{U} define a number conserving correlator so that $[\mathcal{P}_N, \hat{U}] = 0$. We want to compute

$$\frac{\langle \text{AGP} | \hat{U}^\dagger \hat{O} \hat{U} | \text{AGP} \rangle}{\langle \text{AGP} | \text{AGP} \rangle} = \sum_\alpha \lambda_\alpha \frac{|\langle \lambda_\alpha | \hat{V} \hat{U} | \text{AGP} \rangle|^2}{\langle \text{AGP} | \text{AGP} \rangle}, \quad (\text{B3})$$

where \hat{V} diagonalizes \hat{O} , (i.e. $\hat{O} = \hat{V}^\dagger \hat{\Lambda} \hat{V}$) and $|\lambda_\alpha\rangle$ is a bit string corresponding to eigenvector of $\hat{\Lambda}$ with eigenvalue λ_α . In practice, we need to compute Eq. (B3) using the projected BCS wavefunction. Therefore we have

$$\begin{aligned} |\langle \lambda_\alpha | \mathcal{P}_N \hat{V} \hat{U} | \text{BCS} \rangle|^2 &= |\langle \lambda_\alpha | \hat{V} \hat{U} \mathcal{P}_N | \text{BCS} \rangle|^2 \\ &= \underbrace{|\langle \lambda_\alpha | \hat{V} \hat{U} | \text{AGP} \rangle|^2}_{P(\lambda_\alpha|N)} \underbrace{|\langle \text{AGP} | \text{BCS} \rangle|^2}_{P(N)}, \end{aligned} \quad (\text{B4})$$

where $P(N)$ is the probability of getting a state with N pairs and $P(\lambda_\alpha|N)$ is the probability of getting λ_α conditioned on N . This shows that, the scaling of post-selection is solely determined by $P(N)$ and is independent of the operator \hat{O} and the correlator \hat{U} so long as they are number conserving.

From Eq. (B4) we have

$$P(N) = \prod_p u_p^2 \langle \text{AGP} | \text{AGP} \rangle, \quad (\text{B5})$$

where $\langle \text{AGP} | \text{AGP} \rangle = \sum_{1 \leq p_1 < \dots < p_N \leq M} \eta_{p_1}^2 \dots \eta_{p_N}^2 = S_N^M$ is an elementary symmetric polynomial (ESP) [64]. If we did n independent measurements, the probability of getting k observations in the desired particle sector (in the absence of noise) follows a Binomial distribution,

$$P(k; n) = \binom{n}{k} P^k (1 - P)^{n-k}, \quad (\text{B6})$$

where P is a shorthand notation for $P(N)$. Therefore, it follows that

$$P(k \geq 1) = \alpha \implies n = \frac{\log(1 - \alpha)}{\log(1 - P)}. \quad (\text{B7})$$

rounded to the closest integer (ceiling). For example, if we want to be 95% confident that there is at least one observation in the desired particle sector, we need a

sample size of $n = \lceil -2.996/\log(1-P) \rceil$, where P needs to be computed numerically from Eq. (B5).

Finding an upper bound for n is equivalent to bounding P from below. The precise value of P depends on a given Hamiltonian and varies at different correlation regimes; except for special cases, an analytic expressions for P is not known. However, since $0 < P < 1$ we can look at its limiting cases to find the lower and upper bounds.

As $P \rightarrow 1$, we get $n \rightarrow 1$, which corresponds to the HF limit of AGP where fluctuations in particle number are minimal. Indeed this is the upper bound to P . The lower limit corresponds to the opposite case where number symmetry is strongly broken and the number fluctuations are at their peak. Physically, this is associated with the superfluid phase where the occupation number of all orbitals become equal. In this case—assuming $\{\eta_p\}$ normalized so that $\langle \text{BCS} | \hat{N} | \text{BCS} \rangle = 2N$ (*vide supra*)—we get

$$v_p^2 = \frac{N}{M}, \quad u_p^2 = \frac{M-N}{M}, \quad (\text{B8a})$$

$$\eta_p^2 = \frac{N}{M-N}. \quad (\text{B8b})$$

The lower-bound of P can be obtained by plugging these expressions into Eq. (B5), so we arrive at

$$P = \frac{N^N (M-N)^{M-N}}{M^M} \binom{M}{N}. \quad (\text{B9})$$

Using Stirling's approximation,

$$\binom{M}{N} \sim \frac{M^M}{N^N (M-N)^{M-N}} \sqrt{\frac{M}{2\pi N(M-N)}}, \quad (\text{B10})$$

we get

$$P \approx \sqrt{\frac{M}{2\pi N(M-N)}}. \quad (\text{B11})$$

Let $\xi = N/M$ define an intensive quantity. We may assume $\xi \leq 1/2$ for all practical purposes. Simplifying P gives

$$P \approx \frac{1}{\sqrt{2\pi M \xi(1-\xi)}} \geq \frac{1}{\sqrt{\pi M/2}}. \quad (\text{B12})$$

Finally, to get the asymptotic scaling for n , we Taylor expand near $P \rightarrow 0$,

$$n \propto \frac{1}{-\log(1-P)} = \frac{1}{P} - \frac{1}{2} - \frac{P}{12} + \mathcal{O}(P^2), \quad (\text{B13})$$

and plug in Eq. (B12) to obtain

$$n \propto \sqrt{\frac{\pi M}{2}} + \mathcal{O}(P). \quad (\text{B14})$$

This finishes the proof as it shows $n \sim \mathcal{O}(\sqrt{M})$

Appendix C: Implementation details

In Sec. IV, we used PySCF [135] to carry out all UHF and traditional UCCSD calculations. Our quantum algorithms were implemented using the QForte [136] software with the “state-vector” emulator in the absence of noise. We made slight modifications to QForte libraries to implement AGP and orbital rotation/optimization in an in-house code. For the fixed-reference UHF-based calculations, we obtained the molecular orbital coefficients from PySCF; for AGP-based calculations, we used an in-house NHFB code.

For computational feasibility of our quantum algorithms, we implemented AGP by brute force; we looped over all states in the Hilbert space and assigned appropriate coefficients to each state. The procedure can be more easily seen if we expand Eq. (4) to get

$$|\text{AGP}\rangle = \sum_{1 \leq p_1 < \dots < p_N \leq M} \eta_{p_1} \dots \eta_{p_N} \mathbf{P}_{p_1}^\dagger \dots \mathbf{P}_{p_N}^\dagger |\text{vac}\rangle. \quad (\text{C1})$$

For example, for the $M = 4, N = 2$ state, we have

$$\begin{aligned} |\text{AGP}\rangle = & \eta_1 \eta_2 |00001111\rangle + \eta_1 \eta_3 |00110011\rangle \\ & + \eta_1 \eta_4 |11000011\rangle + \eta_2 \eta_3 |00111100\rangle \\ & + \eta_2 \eta_4 |11001100\rangle + \eta_3 \eta_4 |11110000\rangle, \end{aligned} \quad (\text{C2})$$

Note that this state is not normalized, i.e. $\langle \text{AGP} | \text{AGP} \rangle \neq 1$; it is necessary to divide all energy and gradient expressions with appropriate normalization. The gradient with respect to η_p can be computed from [64]

$$\frac{d}{d\eta_p} |\text{AGP}\rangle = \frac{1}{2\eta_p} \mathbf{N}_p |\text{AGP}\rangle. \quad (\text{C3})$$

On a quantum computer, however, we can efficiently compute the gradient by applying the shift-rule to the parameters of the unitary that implements the BCS wavefunction and number projecting the resulting term. This follows from the fact that $\left[\frac{d}{d\eta_p}, \mathcal{P}_N \right] = 0$.

We relied on the existing implementation for ADAPT and VQE calculations which use the SciPy libraries [137] to do the intermediate optimizations. We set the optimizer to be L-BFGS-B [138]; the gradients threshold as well as the energy difference tolerance were set to 10^{-9} . In ADAPT, there is an additional tolerance, ϵ , that determines when it terminates; we set $\epsilon = 10^{-3}$ for the results shown in Fig. (6). In all calculations, the gradients were computed analytically.

To implement orbital rotation, we used an in-house code to perform a QR decomposition in terms of Givens rotations; we followed the work of Ref. [102] closely and implemented the rotations in QForte using 1-body rotations acting on nearest neighbors. For the orbital optimization of Sec. IV B we treated each of these 1-body rotations as independent parameters. Note that care must

be given in making sure spin symmetries are retained. In all of our calculation with orbital optimization, we

made certain that S_z does not break—hence UAGP and UHF—by construction.

-
- [1] Y. Cao, J. Romero, J. P. Olson, M. Degroote, P. D. Johnson, M. Kieferová, I. D. Kivlichan, T. Menke, B. Peropadre, N. P. D. Sawaya, S. Sim, L. Veis, and A. Aspuru-Guzik, *Chem. Rev.* **119**, 10856 (2019).
- [2] S. McArdle, S. Endo, A. Aspuru-Guzik, S. C. Benjamin, and X. Yuan, *Rev. Mod. Phys.* **92**, 015003 (2020).
- [3] T. Helgaker, P. Jørgensen, and J. Olsen, *Molecular electronic-structure theory* (Wiley, Chichester; New York, 2000).
- [4] G. E. Scuseria, A. C. Scheiner, T. J. Lee, J. E. Rice, and H. F. Schaefer, *J. Chem. Phys.* **86**, 2881 (1987).
- [5] R. J. Bartlett and M. Musiał, *Rev. Mod. Phys.* **79**, 291 (2007).
- [6] I. W. Bulik, T. M. Henderson, and G. E. Scuseria, *J. Chem. Theory Comput.* **11**, 3171 (2015).
- [7] P. Ring and P. Schuck, *The Nuclear Many-Body Problem*, Theoretical and Mathematical Physics, The Nuclear Many-Body Problem (Springer-Verlag, Berlin Heidelberg, 1980).
- [8] J.-P. Blaizot and G. Ripka, *Quantum theory of finite systems* (MIT Press, Cambridge, Mass., 1986).
- [9] P.-O. Löwdin, *Phys. Rev.* **97**, 1509 (1955).
- [10] P. Lykos and G. W. Pratt, *Rev. Mod. Phys.* **35**, 496 (1963).
- [11] G. E. Scuseria, C. A. Jiménez-Hoyos, T. M. Henderson, K. Samanta, and J. K. Ellis, *J. Chem. Phys.* **135**, 124108 (2011).
- [12] C. A. Jiménez-Hoyos, T. M. Henderson, T. Tsuchimochi, and G. E. Scuseria, *J. Chem. Phys.* **136**, 164109 (2012).
- [13] F. A. Evangelista, *J. Chem. Phys.* **134**, 224102 (2011).
- [14] T. Duguet, *J. Phys. G: Nucl. Part. Phys.* **42**, 025107 (2015).
- [15] Y. Qiu, T. M. Henderson, J. Zhao, and G. E. Scuseria, *J. Chem. Phys.* **147**, 064111 (2017).
- [16] M. Cerezo, A. Arrasmith, R. Babbush, S. C. Benjamin, S. Endo, K. Fujii, J. R. McClean, K. Mitarai, X. Yuan, L. Cincio, and P. J. Coles, *Nat. Rev. Phys.* **3**, 625 (2021).
- [17] Y. Shen, X. Zhang, S. Zhang, J.-N. Zhang, M.-H. Yung, and K. Kim, *Phys. Rev. A* **95**, 020501 (2017).
- [18] J. Tilly, H. Chen, S. Cao, D. Picozzi, K. Setia, Y. Li, E. Grant, L. Wossnig, I. Rungger, G. H. Booth, and J. Tennyson, *arXiv:2111.05176 [quant-ph]* (2021).
- [19] A. Anand, P. Schleich, S. Alperin-Lea, P. W. K. Jensen, S. Sim, M. Díaz-Tinoco, J. S. Kottmann, M. Degroote, A. F. Izmaylov, and A. Aspuru-Guzik, *Chem. Soc. Rev.* **51**, 1659 (2022).
- [20] F. A. Evangelista, G. K.-L. Chan, and G. E. Scuseria, *J. Chem. Phys.* **151**, 244112 (2019).
- [21] H. R. Grimsley, D. Claudino, S. E. Economou, E. Barnes, and N. J. Mayhall, *J. Chem. Theory Comput.* **16**, 1 (2020).
- [22] A. F. Izmaylov, M. Díaz-Tinoco, and R. A. Lang, *Phys. Chem. Chem. Phys.* **22**, 12980 (2020).
- [23] A. Peruzzo, J. McClean, P. Shadbolt, M.-H. Yung, X.-Q. Zhou, P. J. Love, A. Aspuru-Guzik, and J. L. O’Brien, *Nat. Commun.* **5**, 1 (2014).
- [24] J. R. McClean, J. Romero, R. Babbush, and A. Aspuru-Guzik, *New J. Phys.* **18**, 023023 (2016).
- [25] H. R. Grimsley, S. E. Economou, E. Barnes, and N. J. Mayhall, *Nat. Commun.* **10**, 3007 (2019).
- [26] H. L. Tang, V. Shkolnikov, G. S. Barron, H. R. Grimsley, N. J. Mayhall, E. Barnes, and S. E. Economou, *PRX Quantum* **2**, 020310 (2021).
- [27] H. R. Grimsley, G. S. Barron, E. Barnes, S. E. Economou, and N. J. Mayhall, (2022), [10.48550/ARXIV.2204.07179](https://arxiv.org/abs/10.48550/ARXIV.2204.07179).
- [28] A. M. Romero, J. Engel, H. L. Tang, and S. E. Economou, *Phys. Rev. C* **105**, 064317 (2022).
- [29] I. G. Ryabinkin, T.-C. Yen, S. N. Genin, and A. F. Izmaylov, *J. Chem. Theory Comput.* **14**, 6317 (2018).
- [30] I. G. Ryabinkin, R. A. Lang, S. N. Genin, and A. F. Izmaylov, *J. Chem. Theory Comput.* **16**, 1055 (2020).
- [31] Y. Matsuzawa and Y. Kurashige, *J. Chem. Theory Comput.* **16**, 944 (2020).
- [32] J. Lee, W. J. Huggins, M. Head-Gordon, and K. B. Whaley, *J. Chem. Theory Comput.* **15**, 311 (2019).
- [33] N. H. Stair and F. A. Evangelista, *PRX Quantum* **2**, 030301 (2021).
- [34] A. Kandala, A. Mezzacapo, K. Temme, M. Takita, M. Brink, J. M. Chow, and J. M. Gambetta, *Nature* **549**, 242 (2017).
- [35] P.-L. Dallaire-Demers, J. Romero, L. Veis, S. Sim, and A. Aspuru-Guzik, *Quantum Sci. Technol.* **4**, 045005 (2019).
- [36] R. Xia and S. Kais, *Quantum Sci. Technol.* **6**, 015001 (2020).
- [37] G.-L. R. Anselmetti, D. Wierichs, C. Gogolin, and R. M. Parrish, *New J. Phys.* **23**, 113010 (2021).
- [38] W. J. Huggins, B. A. O’Gorman, N. C. Rubin, D. R. Reichman, R. Babbush, and J. Lee, *Nature* **603**, 416 (2022).
- [39] J. Preskill, *Quantum* **2**, 79 (2018).
- [40] F. Leymann and J. Barzen, *Quantum Sci. Technol.* **5**, 044007 (2020).
- [41] T. Duguet and A. Signoracci, *J. Phys. G: Nucl. Part. Phys.* **44**, 015103 (2017).
- [42] J. M. Wahlen-Strothman, T. M. Henderson, M. R. Hermes, M. Degroote, Y. Qiu, J. Zhao, J. Dukelsky, and G. E. Scuseria, *The Journal of Chemical Physics* **146**, 054110 (2017).
- [43] Y. Qiu, T. M. Henderson, T. Duguet, and G. E. Scuseria, *Phys. Rev. C* **99**, 044301 (2019).
- [44] R. Song, T. M. Henderson, and G. E. Scuseria, *J. Chem. Phys.* **156**, 104105 (2022).
- [45] J. A. Sheikh, J. Dobaczewski, P. Ring, L. M. Robledo, and C. Yannouleas, *J. Phys. G: Nucl. Part. Phys.* **48**, 123001 (2021).
- [46] A. F. Izmaylov, *J. Phys. Chem. A* **123**, 3429 (2019).
- [47] T.-C. Yen, R. A. Lang, and A. F. Izmaylov, *J. Chem. Phys.* **151**, 164111 (2019).
- [48] T. Tsuchimochi, Y. Mori, and S. L. Ten-no, *Phys. Rev. Research* **2**, 043142 (2020).

- [49] K. Seki, T. Shirakawa, and S. Yunoki, *Phys. Rev. A* **101**, 052340 (2020).
- [50] D. Lacroix, *Phys. Rev. Lett.* **125**, 230502 (2020).
- [51] P. Siwach and D. Lacroix, *Phys. Rev. A* **104**, 062435 (2021).
- [52] K. Seki and S. Yunoki, *Phys. Rev. A* **105**, 032419 (2022).
- [53] E. A. Ruiz Guzman and D. Lacroix, *Phys. Rev. C* **105**, 024324 (2022).
- [54] A. Khamoshi, F. A. Evangelista, and G. E. Scuseria, *Quantum Sci. Technol.* **6**, 014004 (2020).
- [55] C. N. Yang, *Rev. Mod. Phys.* **34**, 694 (1962).
- [56] A. J. Coleman, *J. Math. Phys.* **6**, 1425 (1965).
- [57] L. M. Sager and D. A. Mazziotti, *Phys. Rev. Research* **4**, 013003 (2022).
- [58] J. Bardeen, L. N. Cooper, and J. R. Schrieffer, *Phys. Rev.* **108**, 1175 (1957).
- [59] D. M. Brink and R. A. Broglia, *Nuclear Superfluidity: Pairing in Finite Systems*, 1st ed. (Cambridge University Press, 2005).
- [60] A. Sedrakian and J. W. Clark, *Eur. Phys. J. A* **55**, 167 (2019).
- [61] V. Bach, E. H. Lieb, and J. P. Solovej, *J Stat Phys* **76**, 3 (1994).
- [62] P. R. Surján, *Top. Curr. Chem.* **203**, 63 (1999).
- [63] T. M. Henderson and G. E. Scuseria, *J. Chem. Phys.* **151**, 051101 (2019).
- [64] A. Khamoshi, T. M. Henderson, and G. E. Scuseria, *J. Chem. Phys.* **151**, 184103 (2019).
- [65] R. Dutta, T. M. Henderson, and G. E. Scuseria, *J. Chem. Theory Comput.* **16**, 6358 (2020).
- [66] T. M. Henderson and G. E. Scuseria, *J. Chem. Phys.* **153**, 084111 (2020).
- [67] R. Dutta, G. P. Chen, T. M. Henderson, and G. E. Scuseria, *J. Chem. Phys.* **154**, 114112 (2021).
- [68] A. Khamoshi, G. P. Chen, T. M. Henderson, and G. E. Scuseria, *J. Chem. Phys.* **154**, 074113 (2021).
- [69] M. Casula and S. Sorella, *J. Chem. Phys.* **119**, 6500 (2003).
- [70] M. Casula, C. Attaccalite, and S. Sorella, *J. Chem. Phys.* **121**, 7110 (2004).
- [71] H. Wei and E. Neuscamman, *J. Chem. Phys.* **149**, 184106 (2018).
- [72] C. Genovese, A. Meninno, and S. Sorella, *J. Chem. Phys.* **150**, 084102 (2019).
- [73] C. Genovese and S. Sorella, *J. Chem. Phys.* **153**, 164301 (2020).
- [74] E. Neuscamman, *J. Chem. Phys.* **139**, 194105 (2013).
- [75] E. Neuscamman, *J. Chem. Phys.* **139**, 181101 (2013).
- [76] C.-E. Fecteau, F. Berthiaume, M. Khalfoun, and P. A. Johnson, *J. Math. Chem.* (2020).
- [77] P. A. Johnson, C.-E. Fecteau, F. Berthiaume, S. Cloutier, L. Carrier, M. Gratton, P. Bultinck, S. De Baerdemacker, D. Van Neck, P. Limacher, and P. W. Ayers, *J. Chem. Phys.* **153**, 104110 (2020).
- [78] P. A. Johnson, H. Fortin, S. Cloutier, and C.-É. Fecteau, *J. Chem. Phys.* **154**, 124125 (2021).
- [79] C.-E. Fecteau, H. Fortin, S. Cloutier, and P. A. Johnson, *J. Chem. Phys.* **153**, 164117 (2020).
- [80] C.-É. Fecteau, S. Cloutier, J.-D. Moisset, J. Boulay, P. Bultinck, A. Faribault, and P. A. Johnson, *J. Chem. Phys.* **156**, 194103 (2022).
- [81] J.-D. Moisset, C.-É. Fecteau, and P. A. Johnson, *J. Chem. Phys.* **156**, 214110 (2022).
- [82] S. Endo, S. C. Benjamin, and Y. Li, *Phys. Rev. X* **8**, 031027 (2018).
- [83] X. Bonet-Monroig, R. Sagastizabal, M. Singh, and T. E. O'Brien, *Phys. Rev. A* **98**, 062339 (2018).
- [84] A. Kandala, K. Temme, A. D. Córcoles, A. Mezzacapo, J. M. Chow, and J. M. Gambetta, *Nature* **567**, 491 (2019).
- [85] S. Endo, Z. Cai, S. C. Benjamin, and X. Yuan, *J. Phys. Soc. Jpn.* **90**, 032001 (2021).
- [86] W. J. Huggins, J. R. McClean, N. C. Rubin, Z. Jiang, N. Wiebe, K. B. Whaley, and R. Babbush, *npj Quantum Inf* **7**, 23 (2021).
- [87] L.-K. Hua, *Am. J. Math.* **66**, 470 (1944).
- [88] T. M. Henderson, I. W. Bulik, and G. E. Scuseria, *J. Chem. Phys.* **142**, 214116 (2015).
- [89] L. Bytautas, T. M. Henderson, C. A. Jiménez-Hoyos, J. K. Ellis, and G. E. Scuseria, *J. Chem. Phys.* **135**, 044119 (2011).
- [90] T. Stein, T. M. Henderson, and G. E. Scuseria, *J. Chem. Phys.* **140**, 214113 (2014).
- [91] T. M. Henderson, I. W. Bulik, T. Stein, and G. E. Scuseria, *J. Chem. Phys.* **141**, 244104 (2014).
- [92] L. Bytautas, G. E. Scuseria, and K. Ruedenberg, *J. Chem. Phys.* **143**, 094105 (2015).
- [93] J. J. Shepherd, T. M. Henderson, and G. E. Scuseria, *J. Chem. Phys.* **144**, 094112 (2016).
- [94] V. E. Elfving, M. Millaruelo, J. A. Gámez, and C. Gogolin, *Phys. Rev. A* **103**, 032605 (2021).
- [95] A. Veillard and E. Clementi, *Theoret. Chim. Acta* **7**, 133 (1967).
- [96] M. Couty and M. B. Hall, *J. Phys. Chem. A* **101**, 6936 (1997).
- [97] C. Kollmar and B. A. Heß, *J. Chem. Phys.* **119**, 4655 (2003).
- [98] P. Jordan and E. Wigner, *Z. Physik* **47**, 631 (1928).
- [99] Z. Jiang, K. J. Sung, K. Kechedzhi, V. N. Smelyanskiy, and S. Boixo, *Phys. Rev. Applied* **9**, 044036 (2018).
- [100] D. Thouless, *Nucl. Phys.* **21**, 225 (1960).
- [101] R. Balian and E. Brezin, *Nuov. Cim. B* **64**, 37 (1969).
- [102] I. D. Kivlichan, J. McClean, N. Wiebe, C. Gidney, A. Aspuru-Guzik, G. K.-L. Chan, and R. Babbush, *Phys. Rev. Lett.* **120**, 110501 (2018).
- [103] M. Schuld, V. Bergholm, C. Gogolin, J. Izaac, and N. Killoran, *Phys. Rev. A* **99**, 032331 (2019).
- [104] J. S. Kottmann, A. Anand, and A. Aspuru-Guzik, *Chem. Sci.* **12**, 3497 (2021).
- [105] A. F. Izmaylov, R. A. Lang, and T.-C. Yen, *Phys. Rev. A* **104**, 062443 (2021).
- [106] W. Mizukami, K. Mitarai, Y. O. Nakagawa, T. Yamamoto, T. Yan, and Y.-y. Ohnishi, *Phys. Rev. Research* **2**, 033421 (2020).
- [107] I. O. Sokolov, P. K. Barkoutsos, P. J. Ollitrault, D. Greenberg, J. Rice, M. Pistoia, and I. Tavernelli, *J. Chem. Phys.* **152**, 124107 (2020).
- [108] C. Bloch and A. Messiah, *Nucl. Phys.* **39**, 95 (1962).
- [109] J. Egido and P. Ring, *Nucl. Phys. A* **383**, 189 (1982).
- [110] J. A. Sheikh and P. Ring, *Nucl. Phys. A* **665**, 71 (2000).
- [111] M. Nooijen, *Phys. Rev. Lett.* **84**, 2108 (2000).
- [112] A. G. Taube and R. J. Bartlett, *Int. J. Quantum Chem.* **106**, 3393 (2006).
- [113] J. Romero, R. Babbush, J. R. McClean, C. Hempel, P. J. Love, and A. Aspuru-Guzik, *Quantum Sci. Technol.* **4**, 014008 (2018).
- [114] B. O'Gorman, W. J. Huggins, E. G. Rieffel, and K. B.

- Whaley, [arXiv:1905.05118](https://arxiv.org/abs/1905.05118) (2019).
- [115] T. Takeshita, N. C. Rubin, Z. Jiang, E. Lee, R. Babbush, and J. R. McClean, *Phys. Rev. X* **10**, 011004 (2020).
- [116] M. Motta, E. Ye, J. R. McClean, Z. Li, A. J. Minnich, R. Babbush, and G. K.-L. Chan, *npj Quantum Inf* **7**, 83 (2021).
- [117] N. C. Rubin, J. Lee, and R. Babbush, *J. Chem. Theory Comput.* **18**, 1480 (2022).
- [118] J. S. Kottmann and A. Aspuru-Guzik, *Phys. Rev. A* **105**, 032449 (2022).
- [119] R. Babbush, D. W. Berry, J. R. McClean, and H. Neven, *npj Quantum Inf* **5**, 92 (2019).
- [120] T.-C. Yen, V. Verteletskiy, and A. F. Izmaylov, *J. Chem. Theory Comput.* **16**, 2400 (2020).
- [121] A. F. Izmaylov, T.-C. Yen, R. A. Lang, and V. Verteletskiy, *J. Chem. Theory Comput.* **16**, 190 (2020).
- [122] M. A. Nielsen and I. L. Chuang, *Quantum computation and quantum information*, 10th ed. (Cambridge University Press, Cambridge ; New York, 2010).
- [123] Google AI Quantum and Collaborators, F. Arute, K. Arya, R. Babbush, D. Bacon, J. C. Bardin, R. Barends, S. Boixo, M. Broughton, B. B. Buckley, D. A. Buell, B. Burkett, N. Bushnell, Y. Chen, Z. Chen, B. Chiaro, R. Collins, W. Courtney, S. Demura, A. Dunsworth, E. Farhi, A. Fowler, B. Foxen, C. Gidney, M. Giustina, R. Graff, S. Habegger, M. P. Harrigan, A. Ho, S. Hong, T. Huang, W. J. Huggins, L. Ioffe, S. V. Isakov, E. Jeffrey, Z. Jiang, C. Jones, D. Kafri, K. Kechedzhi, J. Kelly, S. Kim, P. V. Klimov, A. Korotkov, F. Kostritsa, D. Landhuis, P. Laptev, M. Lindmark, E. Lucero, O. Martin, J. M. Martinis, J. R. McClean, M. McEwen, A. Megrant, X. Mi, M. Mohseni, W. Mroczkiewicz, J. Mutus, O. Naaman, M. Neeley, C. Neill, H. Neven, M. Y. Niu, T. E. O'Brien, E. Ostby, A. Petukhov, H. Putterman, C. Quintana, P. Roushan, N. C. Rubin, D. Sank, K. J. Satzinger, V. Smelyanskiy, D. Strain, K. J. Sung, M. Szalay, T. Y. Takeshita, A. Vainsencher, T. White, N. Wiebe, Z. J. Yao, P. Yeh, and A. Zalcman, *Science* **369**, 1084 (2020).
- [124] T.-C. Yen and A. F. Izmaylov, *PRX Quantum* **2**, 040320 (2021).
- [125] S. McArdle, X. Yuan, and S. Benjamin, *Phys. Rev. Lett.* **122**, 180501 (2019).
- [126] F. Arute, K. Arya, R. Babbush, D. Bacon, J. C. Bardin, R. Barends, A. Bengtsson, S. Boixo, M. Broughton, B. B. Buckley, D. A. Buell, B. Burkett, N. Bushnell, Y. Chen, Z. Chen, Y.-A. Chen, B. Chiaro, R. Collins, S. J. Cotton, W. Courtney, S. Demura, A. Derk, A. Dunsworth, D. Eppens, T. Eckl, C. Erickson, E. Farhi, A. Fowler, B. Foxen, C. Gidney, M. Giustina, R. Graff, J. A. Gross, S. Habegger, M. P. Harrigan, A. Ho, S. Hong, T. Huang, W. Huggins, L. B. Ioffe, S. V. Isakov, E. Jeffrey, Z. Jiang, C. Jones, D. Kafri, K. Kechedzhi, J. Kelly, S. Kim, P. V. Klimov, A. N. Korotkov, F. Kostritsa, D. Landhuis, P. Laptev, M. Lindmark, E. Lucero, M. Marthaler, O. Martin, J. M. Martinis, A. Maruszyk, S. McArdle, J. R. McClean, T. McCourt, M. McEwen, A. Megrant, C. Mejuto-Zaera, X. Mi, M. Mohseni, W. Mroczkiewicz, J. Mutus, O. Naaman, M. Neeley, C. Neill, H. Neven, M. Newman, M. Y. Niu, T. E. O'Brien, E. Ostby, B. Pató, A. Petukhov, H. Putterman, C. Quintana, J.-M. Reiner, P. Roushan, N. C. Rubin, D. Sank, K. J. Satzinger, V. Smelyanskiy, D. Strain, K. J. Sung, P. Schmitteckert, M. Szalay, N. M. Tubman, A. Vainsencher, T. White, N. Vogt, Z. J. Yao, P. Yeh, A. Zalcman, and S. Zanker, [arXiv:2010.07965 \[quant-ph\]](https://arxiv.org/abs/2010.07965) (2020).
- [127] T. E. O'Brien, S. Polla, N. C. Rubin, W. J. Huggins, S. McArdle, S. Boixo, J. R. McClean, and R. Babbush, *PRX Quantum* **2**, 020317 (2021).
- [128] J. Dukelsky, S. Pittel, and G. Sierra, *Rev. Mod. Phys.* **76**, 643 (2004).
- [129] "Qiskit: An Open-source Framework for Quantum Computing," (2019).
- [130] T. Tsuchimochi, M. Taii, T. Nishimaki, and S. L. Tenno, [arXiv:2205.07097](https://arxiv.org/abs/2205.07097) (2022).
- [131] L. W. Bertels, H. R. Grimsley, S. E. Economou, E. Barnes, and N. J. Mayhall, [arxiv:2207.03063](https://arxiv.org/abs/2207.03063) (2022).
- [132] V. V. Baran and J. Dukelsky, *Phys. Rev. C* **103**, 054317 (2021).
- [133] J. R. McClean, S. Boixo, V. N. Smelyanskiy, R. Babbush, and H. Neven, *Nat. Commun.* **9**, 1 (2018).
- [134] M. Wimmer, *ACM Trans. Math. Softw.* **38**, 1 (2012).
- [135] Q. Sun, T. C. Berkelbach, N. S. Blunt, G. H. Booth, S. Guo, Z. Li, J. Liu, J. D. McClain, E. R. Sayfutyarova, S. Sharma, S. Wouters, and G. K.-L. Chan, *WIREs Comput. Mol. Sci.* **8** (2018), 10.1002/wcms.1340.
- [136] N. H. Stair and F. A. Evangelista, *J. Chem. Theory Comput.* **18**, 1555 (2022).
- [137] P. Virtanen, R. Gommers, T. E. Oliphant, M. Haberland, T. Reddy, D. Cournapeau, E. Burovski, P. Peterson, W. Weckesser, J. Bright, S. J. van der Walt, M. Brett, J. Wilson, K. J. Millman, N. Mayorov, A. R. J. Nelson, E. Jones, R. Kern, E. Larson, C. J. Carey, Í. Polat, Y. Feng, E. W. Moore, J. VanderPlas, D. Laxalde, J. Perktold, R. Cimrman, I. Henriksen, E. A. Quintero, C. R. Harris, A. M. Archibald, A. H. Ribeiro, F. Pedregosa, P. van Mulbregt, SciPy 1.0 Contributors, A. Vijaykumar, A. P. Bardelli, A. Rothberg, A. Hilboll, A. Kloeckner, A. Scopatz, A. Lee, A. Rokem, C. N. Woods, C. Fulton, C. Masson, C. Häggström, C. Fitzgerald, D. A. Nicholson, D. R. Hagen, D. V. Pasechnik, E. Olivetti, E. Martin, E. Wieser, F. Silva, F. Lenders, F. Wilhelm, G. Young, G. A. Price, G.-L. Ingold, G. E. Allen, G. R. Lee, H. Audren, I. Probst, J. P. Dietrich, J. Silterra, J. T. Webber, J. Slavič, J. Nothman, J. Buchner, J. Kulick, J. L. Schönberger, J. V. de Miranda Cardoso, J. Reimer, J. Harrington, J. L. C. Rodríguez, J. Nunez-Iglesias, J. Kuczynski, K. Tritz, M. Thoma, M. Newville, M. Kümmerer, M. Bolingbroke, M. Tartre, M. Pak, N. J. Smith, N. Nowaczyk, N. Shebanov, O. Pavlyk, P. A. Brodtkorb, P. Lee, R. T. McGibbon, R. Feldbauer, S. Lewis, S. Tygier, S. Sievert, S. Vigna, S. Peterson, S. More, T. Pudlik, T. Oshima, T. J. Pingel, T. P. Robitaille, T. Spura, T. R. Jones, T. Cera, T. Leslie, T. Zito, T. Krauss, U. Upadhyay, Y. O. Halchenko, and Y. Vázquez-Baeza, *Nat. Methods* **17**, 261 (2020).
- [138] R. H. Byrd, P. Lu, J. Nocedal, and C. Zhu, *SIAM J. Sci. Comput.* **16**, 1190 (1995).